

A Mobile Robot for Automated Civil Infrastructure Inspection and Evaluation

Luan Van Nguyen, Spencer Gibb, Huy Xuan Pham, and Hung Manh La, *Senior Member, IEEE*

Abstract—The objective of civil infrastructure inspection is to evaluate and periodically perform maintenance. This involves properly collecting data on structures, documenting the data, and analyzing the quantitative inspection data over an extended period of operating time, all in order to maintain the structures properly. Recent research on civil infrastructure inspection is mainly based on manual visual inspections, which are often influenced and limited by a professional inspector’s knowledge and experience. Thus, the accuracy and reliability of their results are affected. These inspection processes require significant individual labor, which can become quite costly as the inspection areas often require traffic to be limited or evacuation of certain business parking areas while the inspections are performed. In this paper, we present a new development of the autonomous mobile robotic system for automated data collection and inspection. A 4 degree of freedom (DoF) arm is designed and developed then integrated with the robot for efficient image capture using both visual and thermal cameras. The robotic system performs crack detection on the collected data using a state-of-the-art method involving convolutional neural networks (CNN), which is validated on a variety of test images. As inspection results, the robot can output several condition maps of the inspected infrastructure including crack map, thermal map and deterioration map to provide the overall picture of the structure health condition. Our robotic system reduces the overall inspection time compared to the current robotic inspection methods. We further validate our data collection process through showing the correlation between the data collected by each sensor in the system.

I. INTRODUCTION

In order to maintain civil infrastructure properly, it is necessary to assess the condition of the infrastructure. Regular inspections are necessary to ensure the health of civil infrastructure and to guarantee the safety of those using it. Inspections can be costly for a variety of reasons, including: the cost of closing the infrastructure during the inspection, the cost of training individuals on the complex equipment/sensors used to inspect the infrastructure, and the cost of ensuring the safety of inspectors during the process.

This work is supported by National Science Foundation under grants: NSF-IIP-I-Corps #1639092, and the National Aeronautics and Space Administration (NASA) under Grant No. NNX10AN23H issued through the Nevada Space Grant. This work is also supported by the U.S. Department of Transportation, Office of the Assistant Secretary for Research and Technology (USDOT/OST-R) under Grant No. 69A3551747126 through INSPIRE University Transportation Center (<http://inspire-utc.mst.edu>) at Missouri University of Science and Technology. The views, opinions, findings and conclusions reflected in this publication are solely those of the authors and do not represent the official policy or position of the USDOT/OST-R, or any State or other entity.

The authors are with the Advanced Robotics and Automation (ARA) Lab, Department of Computer Science and Engineering, University of Nevada, Reno, NV 89557, USA.

Corresponding author: Hung La (e-mail: hla@unr.edu).

Not only is the inspection process costly, it is also time consuming and heavily influenced by the accuracy, training, and expertise of the person performing the inspection.

Previous work has indicated, the speed, accuracy, and reliability of results all increase as a result of implementing autonomous robotic systems for civil infrastructure inspection tasks [1]–[4]. In this research, we develop an efficient, reliable data collection and inspection robot, which is capable of speeding up the inspection process compared to the current robotic inspection methods. The designed robotic system is integrated with NDE sensors consisting of ground penetrating radar (GPR), electrical resistivity (ER) and thermal camera, and high resolution visual camera. The NDE-based inspection has been known to show correlation with visual inspection methods [5]. The visual inspection can be applied to speed up multi-functional inspection robots, such as the system in [6]. Visual inspection is performed using two kinds of images, high resolution images from a Canon digital single-lens reflex (DSLR) camera, and thermal images from a Flir thermal camera. These two cameras are mounted on the 4 degree of freedom (DoF) arm to allow the robot to efficiently capture high resolution visual and thermal images of the surface of the inspection area during this arm’s movement. At a certain traveling distance (e.g., 3 meters), individual visual images are stitched together, and then analyzed by the robot to detect cracks using a state-of-the-art convolutional neural network (CNN). Thermal images are processed and plotted to visualize a thermal condition map of the surface. Detected cracks from stitched images are used to construct a crack map. The inspection mode of the robotic system then depends on the correlation between individual maps. GPR is used to generate a ground truth attenuation condition map, which serves to validate the results from the visual inspection. The developed robotic system is also equipped with global positioning system (GPS), and an inertial measurement unit (IMU), which are fused with odometry data using Extended Kalman Filter (EKF) [7] to allow the robot to accurately localize and navigate on the inspection area. In summary, the main contributions of the proposed method include: a newly designed arm for faster and more efficient data collection with the robotic system, the addition of a thermal camera as an NDE sensor, increased inspection speed when compared with our previous robotic system in [1], [6], [8], and the introduction of a CNN for crack detection on the robotic system.

The remainder of this paper is organized as follows: in section II, we briefly present the robot’s mechanical arm design and the visual field of the attached cameras. Section

III describes the crack detection implementation on the developed robotic system. In section IV, we present experimental results to validate the robotic inspection system. In section V, a conclusion is given and a discussion of future work is provided.

II. ROBOT SYSTEM ARCHITECTURE

The general architecture of the robotic system is shown in Figure 1. It has a module controlling the movement of the NDE sensors (GPR, ER sensors, and thermal camera), high-resolution Canon camera, water tank solenoid (responsible for dispensing water for the ER sensors), and linear actuators through an Arduino micro-controller and a relay board. It also has a module doing localization and navigation for EKF sensor fusion. In addition, the overall system consists of a wireless connection between the robot and human operator for optional manual control and monitoring of the system.

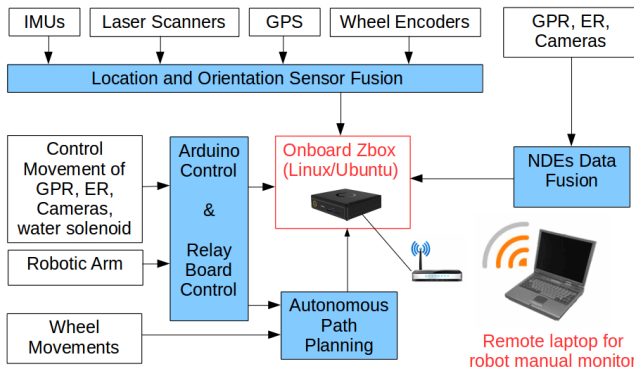


Fig. 1: Architecture of the inspection robotic system.

There have been several publications based on robotic civil infrastructure inspection systems [3], [4], [6], [9], [10]. These methods applied high resolution visual cameras to capture images of varying concrete surfaces. Based on the collected data, crack detection is typically performed, and the results are used to build a condition map of the inspection area. However, most of the previous methods utilized a fixed camera system, which has limitation since the camera only covers a certain area at a time and causes the inspection speed greatly decreased. One example of such a system is the RABIT robotic system [11], in which two cameras are fixed on the front of this robot. As a result, the RABIT system takes approximately 33 minutes to collect visual data on a bridge scan area of 10.67 meters by 1.07 meters [11], [12]. Such a system requires considerable inspection time as the size of the inspection area increases, which can lead to costly inspections.

There has been some research applying thermal cameras for inspection of concrete bridge decks [13], [14] since they can detect delamination of concrete structures. However, these cameras are manually used and thus their data is manually processed. This motivates us to equip this thermal camera on our inspection robot to automate the data collection and processing, which is a significant new addition to our robotic inspection system as it has not been deployed for

inspection in previous research. We use a Flir A3XX/SC3XX Series thermal camera in this research. This thermal camera specifications are as follows: horizontal field of view (HFOV) of 25°, focal length of 18.04 mm, close focus limit of 0.40 meters, f -number of 1.3. The limited field of view of the thermal camera requires the camera to be lifted up above the ground as high as possible to get as much of the inspection area in each scan as possible, which has motivated our research to design a new robotic arm for the intelligent inspection system to facilitate efficient visual data collection.

A. 4 DoF Robotic Arm Mechanic Design

We design and implement a robotic arm to enable the image collection using both a visual camera and a thermal camera. The weight of both the Canon T3i and Flir A3XX cameras and their frame is about 11.34 kg. Our developed robotic arm that has 4 DoF of movement can hold both camera components stably during the robotic system's movement and scanning. When the robotic arm raises up to maximum level, the thermal camera is about 1.67 meters off the ground, allowing it to capture an area of 0.73×0.55 sq. meters.

The designed robotic arm attaches to the top-front of the robotic system, as in Figure 2. Its functions are to lift the cameras up and down, and to allow them to have 2 DoF to scan from left to right. The arm has two segments, which can fold up to 90° or fold down to 60° using two linear actuators, as in Figure 2 (a) and (b). We use several ports on a relay board to control the motion of each linear actuator during operation through Robotic Operating System (ROS) drivers. When the arm folds down, it allows the robot to maneuver easily in hallways and in other narrow spaces. Each segment is 1.22 meters long, so the arm can extend the cameras up to 1.67 meters, and 1.22 meters in front of robot.

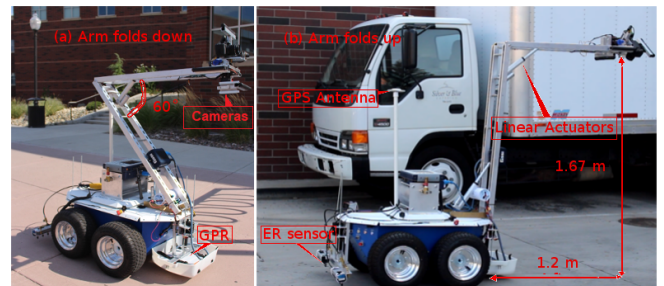


Fig. 2: Robotic arm.

At the end of the robotic arm is a camera component, which mounts a high resolution image Canon T3i, a Flir thermal camera and one low resolution web camera. This 2 DoF component's rotation is controlled by two servo motors, which are controlled by an Arduino micro-controller using ROS drivers. They allow cameras to rotate 90° vertically and swing 135° horizontally, as in Figure 3.

Around the camera component, we mounted 4 electric bumpers to protect this component physically, as in Figure 4 (b). These bumpers will stop the robot's movement in case of a collision with obstacle.

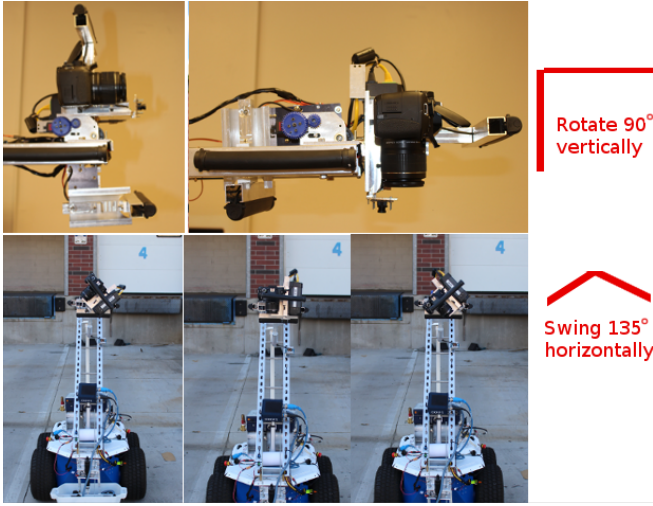


Fig. 3: 2DoF camera component.

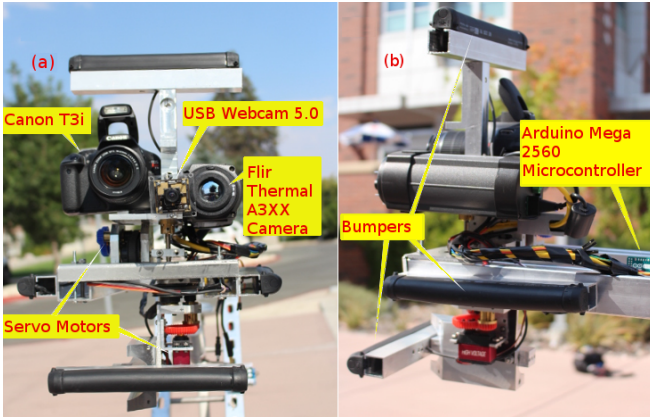


Fig. 4: Camera Component of the robotic arm.

B. Robot Visual View

Using the robot arm designed above, in each scanning step the robot can capture 10 overlapping images from both the normal and thermal cameras. The images are captured between the beginning position at 202° and the ending position at 337° in the Cartesian coordinate system, such as in Figure 5.

Where, I_{ci} $i = 1..10$ is center of image i .

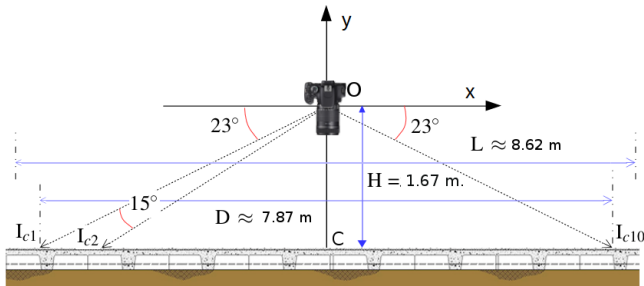


Fig. 5: Camera scanning field.

Each captured image is positioned 15° farther than the previous one. Thus, the robot collects 10 overlapping images for each panoramic image scan. The center point of each image is labeled by I_{ci} , where c is a symbol of image center,

and subscript i is an image index, $i \in \{1, \dots, 10\}$. We call height of camera position H ($H = 1.67$ meters in this case), then the distance D between the center of the first image I_{c1} and the center of the last image I_{c10} of scanning field is computed by Equation (1).

$$D = 2 \times I_{c1}C = 2 \times H \times \tan(67^\circ) = 2 \times 1.67 \times 2.35 \approx 7.87m. \quad (1)$$

At a height of 1.67 meters, the designed arm allows the thermal camera to have a fixed capture area of 0.75×0.55 sq. meters, so that satisfies the Flir A3XX specification. Given this layout, the total length of the scanning field of these cameras is computed by Equation (2).

$$L \approx 7.87m. + 0.75m. \approx 8.62m. \quad (2)$$

The function of our panoramic collection and stitching is similar to that of the camera systems by GigaPan [15], but at no additional cost to that of the original camera.

C. Ground-penetrating Radar

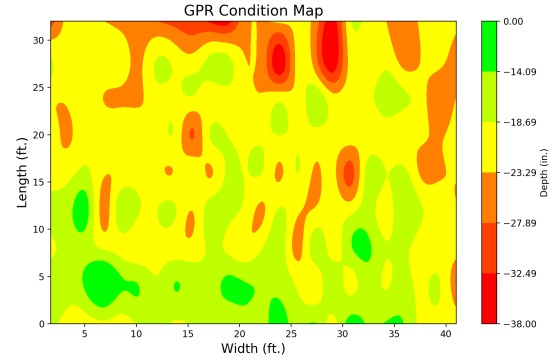


Fig. 6: GPR deterioration condition map of the entire inspection area generated by the robot: red areas indicate serious/bad condition of the concrete structure; yellow color indicates average condition; blue and green colors indicates good to excellent condition. Inspection was performed in a U-shape pattern using IMU and odometry data, as well as the dimensions of the inspection area.

In addition to visual and thermal data, the robot collects GPR data. GPR can detect buried metal objects, including steel rebar, which serve to reinforce concrete [16]. The algorithm used to locate steel rebar in GPR scan images can be seen in [17]. The rebar detection results are used to generate an attenuation condition map of the inspected area. This condition map is represented as colored contour plots to visualize the condition of rebar underneath the inspected surface. As seen in Fig.6, green areas indicate that the rebar beneath the concrete are in good condition, yellow areas are in questionable (unknown whether these areas are in normal or poor condition) condition, and red areas are in poor condition (rebar may be corroded).

III. CRACK DETECTION USING A CONVOLUTIONAL NEURAL NETWORK

Crack detection in concrete and pavement has been attempted with many image processing, computer vision, and machine learning techniques. Initial attempts to detect

cracks in images of concrete were performed using methods such as the Canny edge detector, Sobel filter, Laplace of Gaussian (LoG) [2], [18] for edge detection, and other simple methods. These methods do not perform well in cases where the images are noisy, have shadows, or have textured backgrounds [19]. In an attempt to improve crack detection accuracy compared to these classic methods, newer modeling and learning techniques have been applied to crack detection in recent research. Among these techniques are random forest classifiers, neural networks, percolation-based edge detection, and frequency domain filtering [11], [20]–[22]. While modern work tends to show high accuracy in crack classification, various models and techniques more or less accurately depending on the test environment, camera system, lighting, the presence of other objects in the image, and the size and depth of cracks in the test images [23].

Our developed robotic system is capable of collecting data from several sensors, including the equipped DSLR camera. This camera captures images at the same time as the equipped thermal camera system. After these images have been stitched together to form a large image of the local inspection area, crack detection is performed on the robotic system through the use of a CNN that was trained with this task in mind. This is a new addition to our robotic inspection system and performs more accurate detection than the methods employed in our previous work [6].

A. Network Structure

In order for the structure of the implemented CNN to be explained, a simple overview of the core CNN concepts is provided. There are three main types of layers that are part of the network: convolution layers, pooling layers, and activation layers. Each layer has a specific function that contributes to the overall success of the network in this classification task.

Convolution layers perform element-wise multiplication followed by addition between the input image and a set of filters. These filters are updated throughout the training process, which changes the way that samples are represented through both the training and testing processes. Pooling layers take the results from a set of convolutions and combine them according to their type. In the case of maximum pooling, the pooling process takes the maximum value output in an area during the convolution process, whereas average pooling takes the average of values output by convolutions in that same respective area. After convolution and pooling layers are applied to the network, activation layers are applied to introduce non-linearity to the network. More information on these layer types and their functionality can be seen in [24]. Information on the general network structure optimization (filter sizes, number of filters, and input/output size) can be found in [25].

B. Training and Classification

In order to train the implemented network, training images were divided into 256 by 256 pixel sub-images and manually labeled as a part of the *crack* class or as part of the *no-crack*

class. Images containing no cracks were plentiful during the labeling process, so the total number of images in each class was limited to 4,000 to keep the number of training images equal for both classes. It should be noted that this is far less training examples than the number used in [24], due to the time required to collect crack data and manually label it. The lack of training images results in inferior classifier performance, but the performance of the classifier is ample for the task at hand, as is shown in the experimental results section. Given more time and resources in the future, it would benefit the classifier to increase the number of training samples.

The CNN was trained across 30 epochs, where each epoch the weights of the network are modified in an attempt to maximize the validation accuracy of the classifier. This process can be lengthy depending on the training hardware, but can be done off-line. The speed of this process can be greatly improved with the use of a graphics processing unit (GPU).

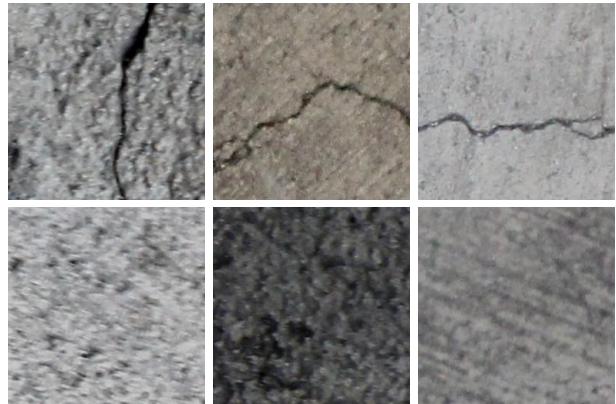


Fig. 7: Training images belonging to the *crack* class (top) and training images belonging to the *no-crack* class (bottom).

As seen in Figure 7, training images consisted of those with clear centered cracks in them, and those without any cracks, which belong to the *no-crack* class.

C. Crack Detection Experimental Results

To verify the performance of the trained classifier, multiple test images were run. The classification process consists of a sliding window approach, where the entire image is covered to ensure all areas are classified. The reader is directed to [24], [25] for further information.

As can be seen in Figure 8, the classifier was tested on images with clear cracks, but heavy background variation, including oil spots, water spills, and even spalling concrete. Despite the fact that the classifier has not seen any of these things before, it performs well in all of these test cases. The classifier was also tested on an image containing no cracks, which is shown in the bottom of Figure 8. This case resulted in very few false positives despite the numerous oil spots in the image, which would cause false detections to happen when analyzed by many of the previously discussed methods. A table showing the complete test results of the classifier on several thousand test images is shown in Table I. For further

# of Images Tested	Correct Classifications	Incorrect Classifications	Accuracy (%)	False Positives	False Negatives
2440	2188	252	89.67	232	20

TABLE I: Table of CNN crack detection results.

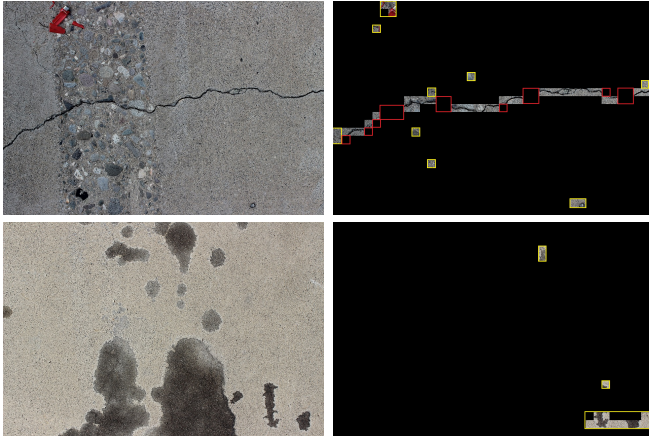


Fig. 8: Training results of two cases: a crack with background concrete spalling (top), and a case with no cracks but significant oil stains on the background (bottom). False positives are surrounded by red rectangles, and false negatives are surrounded by yellow rectangles.

results using the network implemented here, the reader is encouraged to check out the extensive results in [24], [25].

IV. SYSTEM VALIDATION

In order to test and validate the performance of our developed robotic system, we deploy it on a concrete truck docking station at UNR campus. This docking station has a $12.19m. \times 16.76m.$ area, as shown in Figure 9, and is divided into 3 lanes, each 3.96 m. wide. In each scan, the robot can cover a width of 6.1 m. To cover the entirety of this inspection area the robot takes two scanning lines in a U shape trajectory, represented by the green line in Figure 9.

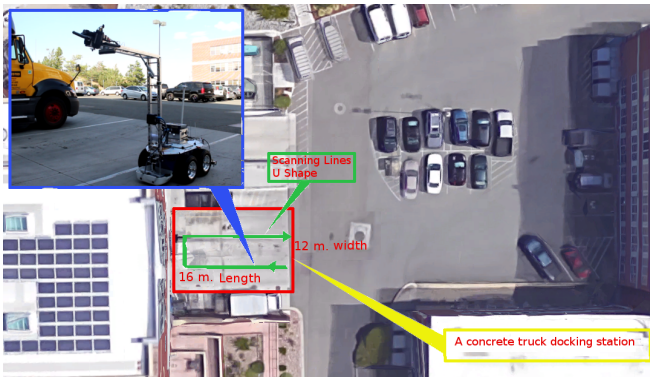


Fig. 9: Deployment of the robot on the truck dock station at UNR campus.

The general workflow of data analysis and map fusion is explained in Figure 10. The robot collects visual images and thermal images and then stitches them together. The visual image stitching algorithm is implemented on board the robot using C++, in Open CV 3.1, running on ROS, so the robot

can stitch images together after the CNN is applied, to help build a crack map.

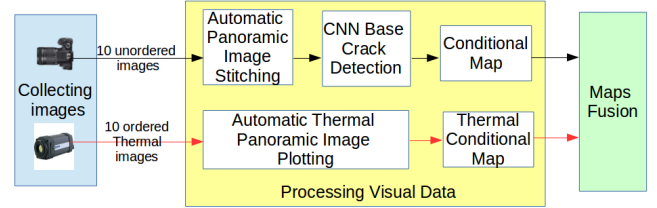


Fig. 10: Processing data and fusion diagram.

Individual thermal images are also stitched together for the ease of visualization of condition map. In the Figure 11, we plot the condition maps on the same coordinate system to easily compare and validate the condition of the inspected concrete structure. Based on the crack map and thermal map, we can observe the correlation between detected cracks and thermal source changing on the surface of inspection area. The areas with crack usually lead to delamination (plotted in red color in thermal map) since crack can create a pathway for concrete to absorb salt and water faster and results delamination and spalling of concrete.

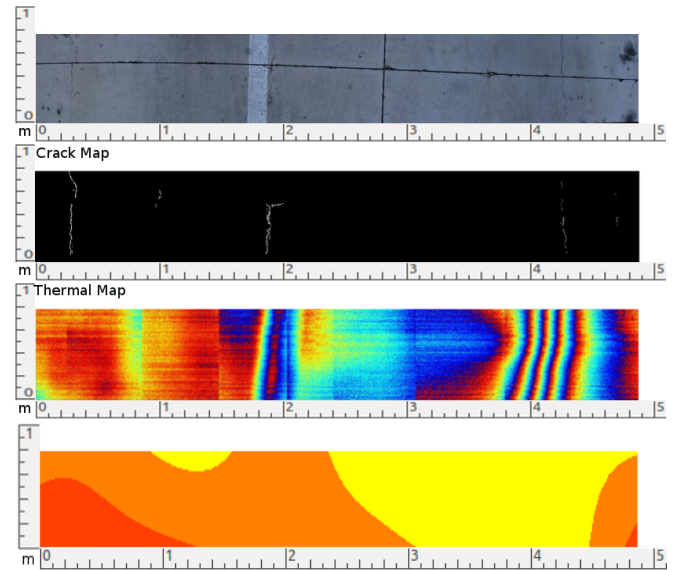


Fig. 11: Multiple condition maps of the concrete area generated by the robot during inspection. (First, from top) Stitched image of the inspection area; (Second) Crack map detected from the stitched image; (Third) Thermal map of the inspection area showing the delamination level of concrete (red: serious condition, yellow-green: average condition, blue: good condition); and (Fourth) Deterioration map from GPR (red: serious condition, orange: average condition, and yellow: good condition). We can clearly see that crack areas are well correlated with delamination (in thermal map) and deterioration (in GPR map): deep/large crack areas lead to serious delamination/deterioration of concrete.

Inspection Timing: At 1.67 meters above the ground and

spanning 135° horizontally, the cameras can scan approximately 6.1 m. × 0.61 m., or 3.72 sq. m. in front of the robot. The thermal camera and Canon T3i have high-speed capture modes, which allow capturing 30 frames per second. Therefore, the robot takes just 35 seconds to perform each scan. The time required to move the robot 0.61 m. is 25 seconds, bringing the total scan time to approximately 60 seconds. The entire area in Figure 9 can be scanned in 20 minutes total. This inspection time is significantly faster than the results in [26], [27], as well as 48.2% faster than our previous robotic inspection system in [6].

V. CONCLUSION AND FUTURE WORK

In this paper, we presented a new development of an autonomous robotic system for civil infrastructure inspection and evaluation. The robot is equipped with multiple NDE sensors (GPR, ER) and thermal/visual cameras associated with the data processing algorithms. The 4 DoF arm is designed and integrated with the robot to enable efficient visual and thermal data collection. The CNN-based crack detection algorithm is proposed and implemented onboard the robot and demonstrates the better performance compared to the existing methods. The proposed robotic system is validated through inspection of a concrete truck docking station, and it can perform high-speed inspection comparing to the previous robotic systems. In the future, this robotic system can be enhanced with a NDE data-driven path planning algorithm. In order to further evaluate and enhance the robot's performance, we plan to vigorously conduct more field testings on other civil infrastructure such as airport runways, sea ports, and bridge decks.

REFERENCES

- [1] T. D. Le, S. Gibb, N. H. Pham, H. M. La, L. Falk, and T. Berendsen, "Autonomous robotic system using non-destructive evaluation methods for bridge deck inspection," in *Robotics and Automation (ICRA), 2017 IEEE International Conference on*. IEEE, 2017.
- [2] R. S. Lim, H. M. La, and W. Sheng, "A robotic crack inspection and mapping system for bridge deck maintenance," *IEEE Transactions on Automation Science and Engineering*, vol. 11, no. 2, pp. 367–378, April 2014.
- [3] N. Gucunski, S. H. Kee, H. M. La, B. Basily, A. Maher, and H. Ghasemi, "Implementation of a fully autonomous platform for assessment of concrete bridge decks rabbit," *Structures Congress, April 23-25, 2015, Portland, Oregon, USA*, pp. 367–378, 2015.
- [4] H. M. La, N. Gucunski, K. Dana, and S.-H. Kee, "Development of an autonomous bridge deck inspection robotic system," *Journal of Field Robotics*, vol. 34, no. 8, pp. 1489–1504. [Online]. Available: <https://onlinelibrary.wiley.com/doi/abs/10.1002/rob.21725>
- [5] N. Gucunski, J. Y. Kim, K. Dinh, T. Duong, and R. Zobel, "Similarities and differences in condition assessment of concrete bridge decks by visual inspection and nde," in *NDE/NDT for Highways and Bridges*, Aug 29 2016.
- [6] S. Gibb, T. D. Le, H. M. La, R. Schmid, and B. Tony., "A multi-functional inspection robot for civil infrastructure evaluation and maintenance." In *Proceedings of the 2017 IEEE/RSJ International Conference on Intelligent Robots and Systems (IROS), September 24-28, 2017, Vancouver, Canada.*, Sept 24-28 2017.
- [7] H. M. La, R. S. Lim, B. B. Basily, N. Gucunski, J. Yi, A. Maher, F. A. Romero, and H. Parvardeh, "Mechatronic systems design for an autonomous robotic system for high-efficiency bridge deck inspection and evaluation," *IEEE/ASME Transactions on Mechatronics*, vol. 18, no. 6, pp. 1655–1664, Dec 2013.
- [8] S. Gibb, H. M. La, T. Le, L. Nguyen, R. Schmid, and H. Pham, "Nondestructive evaluation sensor fusion with autonomous robotic system for civil infrastructure inspection," *Journal of Field Robotics*, vol. 0, no. 0. [Online]. Available: <https://onlinelibrary.wiley.com/doi/abs/10.1002/rob.21791>
- [9] P. Prasanna, K. J. Dana, N. Gucunski, B. B. Basily, H. M. La, R. S. Lim, and H. Parvardeh, "Automated crack detection on concrete bridges," *IEEE Transactions on Automation Science and Engineering*, vol. 13, no. 2, pp. 591–599, April 2016.
- [10] M. Salman and V. Baporikar, "Image based detection and inspection of cracks on bridge surface using an autonomous robot." *International Journal on Recent and Innovation Trends in Computing and Communication*, 2015.
- [11] P. Prasanna, K. J. Dana, N. Gucunski, B. B. Basily, H. M. La, R. S. Lim, and H. Parvardeh, "Automated crack detection on concrete bridges," *IEEE Transactions on Automation Science and Engineering*, vol. 13, no. 2, pp. 591–599, April 2016.
- [12] H. M. La, N. Gucunski, S. H. Kee, and L. Nguyen, "Visual and acoustic data analysis for the bridge deck inspection robotic system," *The 31st International Symposium on Automation and Robotics in Construction and Mining (ISARC)*, July 9-11 2014.
- [13] S. A. Dabous, S. Yaghi, S. Alkass, and O. Moselhi, "Concrete bridge deck condition assessment using ir thermography and ground penetrating radar technologies," *Automation in Construction*, vol. 81, no. Supplement C, pp. 340 – 354, 2017.
- [14] J. Huh, Q. H. Tran, J. H. Lee, D. Y. Han, J. H. Ahn, and S. Yim, "Experimental study on detection of deterioration in concrete using infrared thermography technique," *Advances in Materials Science and Engineering*, vol. 2016, p. 12, 2016.
- [15] "GigaPan," <http://www.gigapan.com>, accessed: 2018-4-29.
- [16] K. Dinh, N. Gucunski, J. Y. Kim, T. Duong, and H. M. La, "Attenuation-based methodology for condition assessment of concrete bridge decks using gpr," in *The 32st International Symposium on Automation and Robotics in Construction and Mining (ISARC), Oulu, Finland, June 15-18 2015*, pp. 1–8.
- [17] S. Gibb and H. M. La, *Automated Rebar Detection for Ground-Penetrating Radar*. Advances in Visual Computing: 12th International Symposium, ISVC 2016, Las Vegas, NV, USA, December 12-14, 2016, Proceedings, Part I: Springer International Publishing, 2016, pp. 815–824.
- [18] R. S. Lim, H. M. La, Z. Shan, and W. Sheng, "Developing a crack inspection robot for bridge maintenance," in *2011 IEEE International Conference on Robotics and Automation*, May 2011, pp. 6288–6293.
- [19] G. T. Shrivakshan and C. Chandrasekar, "A comparison of various edge detection techniques used in image processing," *Int. J. of Computer Science Issues (IJCSI)*, vol. 9, no. 5, pp. 269–276, 09 2012.
- [20] T. H. Dinh, Q. P. Ha, and H. M. La, "Computer vision-based method for concrete crack detection," in *the 14th International Conference on Control, Automation, Robotics and Vision (ICARCV)*, Nov 2016.
- [21] T. Yamaguchi and S. Hashimoto, "Improved percolation-based method for crack detection in concrete surface images," in *2008 19th International Conference on Pattern Recognition*, Dec 2008, pp. 1–4.
- [22] S. Dorafshan, "Comparing automated image-based crack detection techniques in spatial and frequency domains," in *The 26th ASNT Research Symposium*, March 2017.
- [23] S. Dorafshan, M. Maguire, N. V. Hoffer, and C. Coopmans, "Challenges in bridge inspection using small unmanned aerial systems: Results and lessons learned," in *2017 International Conference on Unmanned Aircraft Systems (ICUAS)*, June 2017, pp. 1722–1730.
- [24] Y.-J. Cha, W. Choi, and O. Bykztrk, "Deep learning-based crack damage detection using convolutional neural networks," *Computer-Aided Civil and Infrastructure Engineering*, vol. 32, no. 5, pp. 361–378, 2017. [Online]. Available: <http://dx.doi.org/10.1111/micc.12263>
- [25] S. Gibb, H. M. La, and S. Louis., "A genetic algorithm for convolutional network structure optimization for concrete crack detection," in *Proceedings of the 2018 IEEE Congress on Evolutionary Computation (IEEE CEC)*, July 2018.
- [26] D. Borrmann, F. Leutert, K. Schilling, and A. Nchter, "Fault localisation of electrical equipments using thermal imaging technique," *Control, Automation, Robotics and Vision (ICARCV), 2016 14th International Conference*, Nov 13-15 2016.
- [27] H. M. La, N. Gucunski, S. H. Kee, J. Yi, T. Senlet, and L. Nguyen, "Autonomous robotic system for bridge deck data collection and analysis," *IEEE International Conference on Intelligent Robots and Systems (IROS)*, Sept 14-18 2014.